Measuring Coseismic Displacements With Point-Like Targets Offset Tracking

Xie Hu, Teng Wang, and Mingsheng Liao

***Abstract*—Offset tracking is an important complement to measure large ground displacements in both azimuth and range dimensions where synthetic aperture radar (SAR) interferometry is unfeasible. Subpixel offsets can be obtained by searching for the cross-correlation peak calculated from the match patches uniformly distributed on two SAR images. However, it has its limitations, including redundant computation and incorrect estimations on decorrelated patches. In this letter, we propose a simple strategy that performs offset tracking on detected point-like targets (PT). We first detect image patches within bright PT by using a sinc-like template from a single SAR image and then perform offset tracking on them to obtain the pixel shifts. Compared with the standard method, the application on the 2010 M 7.2 El Mayor–Cucapah earthquake shows that the proposed PT offset tracking can significantly increase the cross-correlation and thus result in both efficiency and reliability improvements.**

***Index Terms*—Offset tracking, point-like targets, synthetic aperture radar interferometry (InSAR).**

I. Introduction

SYNTHETIC aperture radar interferometry (InSAR) has been widely applied in monitoring natural hazards due to its large spatial coverage and all-weather capability. InSAR is able to measure surface displacements along the line-of-sight (LOS) direction with an accuracy of a fraction of the radar wavelength. Although this limitation can be partially resolved through the use of Multiple Aperture InSAR (MAI) technique [1], coherence would get lost when the gradient of displacements exceeds half a fringe per pixel [2]. In other words, when dense fringes appear locally due to large displacement gradients, e.g., near to an earthquake rupture, the coseismic interferograms (also from MAI) may be totally decorrelated. Even though the phase information can be preserved, the unwrapping procedure, which has to be carried out before obtaining the displacement fields, is very challenging in such cases. Additionally, interferometric phase can be affected by tropospheric delays that may require corrections using auxiliary data [3].

On the other hand, offset tracking method offers an alternative way to extract large displacements where the coherence is almost lost due to large deformation gradient, e.g., glacier motion, landslide motion, dune migration, coseismic deformation, etc. This technique was firstly applied on optical images [4], and then on SAR data to map the coseismic displacements in the 1992 Landers earthquake [2], [5]. The core idea of offset tracking is the cross-correlation algorithm, which obtains pixel offsets between the extended match patches from two SAR amplitude images. At first, the initial offsets of the match patches between the master and slave images are calculated from the orbital information. Then, a normalized cross-correlation surface is computed as an indicator of the speckle-pattern similarity between the reference window and a series of same-sized patches within each search window. Subpixel offsets can be determined by searching for the peak of the oversampled correlation surface. The pixel-offset accuracy can be approximately expressed as [6]

$$\sigma = \sqrt{\frac{3}{2N}} \frac{\sqrt{1-\gamma^2}}{\pi\gamma} \tag{1}$$

where σ is the standard deviation (STD) of the pixel-offset estimation error in the unit of pixel, N is the number of samples in the estimation window, and γ is the cross-correlation. The accuracy expression for the incoherent tracking should be similar but with a factor of $\sqrt{2}$ since only half of the information is used [6]. It is evident from (1) that in order to reduce σ, we need a higher cross-correlation and more samples in the estimation window. Given a high cross-correlation (close to 1), the precision in the offset fields can be up to 1/20 of one single-look pixel [7]. As for ASAR data, the azimuth pixel spacing is $\sim$4 m, implying that the estimation error is on the order of $\sim$20 cm. Despite being less accurate than InSAR technique, offset tracking can be very useful when mapping large displacements such as coseismic events [8] and volcano activities [9]. In addition, the acquired offsets provide displacement measurements in two directions, and thus the north–south motions can be recovered from the azimuth offsets. In particular, it allows us to obtain the 3-D displacement fields when ascending and descending data are available [10]. Moreover, the phase unwrapping procedure can be avoided.

However, high relative Doppler centroids, large spatial baselines, and long temporal intervals contribute to the loss of cross-correlation. For such cases, matching those patches that are uniformly distributed throughout the whole scene in the standard offset tracking method may lead to incorrect estimations. Besides, calculating a huge number of extended patches would be time-consuming and therefore sometimes we have to reduce the number of samples in the estimation window as well as the oversample factors when searching for the peak of a cross-correlation surface. Nevertheless, high amplitude cross-correlation can be expected from point-like targets (PT), such as buildings, bare rocks, etc., implying more accurate estimations [6], [11], [12]. In this paper, instead of calculating cross-correlation on uniformly distributed match patches, we first detect image patches within bright PT

Manuscript received August 17, 2012; revised February 25, 2013; accepted March 25, 2013. Date of publication June 11, 2013; date of current version November 8, 2013. This work was supported in part by the National Key Basic Research Program of China under Grant 2013CB733205, the National Natural Science Foundation of China under Grants 41271457 and 41021061, the National High Technology Research and Development Program of China under Grant 2011AA120404, and the Research Fund for the Doctoral Program of Higher Education of China under Grant 20110141110057.

X. Hu and M. Liao are with the State Key Laboratory of Information Engineering in Surveying, Mapping, and Remote Sensing, Wuhan University, Wuhan 430079, China (e-mail: xiehu@whu.edu.cn; liao@whu.edu.cn).

T. Wang is with the Division of Physical Sciences and Engineering, King Abdullah University of Science and Technology, Thuwal 23955-6900, Saudi Arabia (e-mail: wang.teng@gmail.com).

Color versions of one or more of the figures in this paper are available online at http://ieeexplore.ieee.org.

Digital Object Identifier 10.1109/LGRS.2013.2256104

candidates using a sinc-like template and then perform offset tracking on them to obtain the pixel offsets. This method is referred to as PT offset tracking. A similar strategy was first used in multi-pass SAR data coregistration [11], [12]. Obviously, PT detection and PT offset tracking are two steps for this method. Adaptive thresholds are used to get a balance between the number of PT and the accuracy of offsets when selecting the PT candidates. Then the pixel offsets are estimated similar to the standard offset tracing.

The proposed PT offset tracking was applied on 2010 M7.2 El Mayor–Cucapah earthquake, and then was compared with standard offset tracking results. A clear discontinuity in surface displacements due to fault slip can be identified in the offset fields by both methods. However, since the cross-correlation between SAR images is calculated on the selected match patches, higher cross-correlation, namely higher level offset accuracy can be expected from PT offset tracking. Thanks to the reduced data redundancy, the computational efficiency of amplitude cross-correlation is also highly improved compared to the standard method. Moreover, because less match patches are used than in standard offset tracking, we can also use larger oversampling factors when locating the peak on the cross-correlation surface and therefore further improve the accuracy of the displacement measurements. Finally, more measurements can be kept after outlier removal, leading to more robust subsampling results.

II. PT Detection and Offset Tracking

In time-series InSAR techniques, such as Persistent Scatterer InSAR (PS-InSAR), PS candidates, i.e., PT are detected by the amplitude dispersion [13]. However, this strategy is based on amplitude statistical analysis that requires a certain number of SAR images. As for coseismic studies, we often have only a couple of images, i.e., acquired before and after the event. As a consequence, the PT match patches need to be detected from a single SAR image.

High amplitude values should be the first consideration for PT detection. However, bright pixels may result from the fore-shortening effect in mountainous areas. Besides, the side lobe of a strong PT may also cause some pseudo PT candidates nearby. Therefore, we need to simultaneously consider the amplitude and the reflectivity characteristics of each PT. Since the signal reflected from an ideal PT behaves as a 2-D sinc function [12], we can calculate the cross-correlation between the master image and an ideal sinc-like 2-D impulse response function. The 2-D cross-correlation can be achieved by many signal processing tool boxes. The cross-correlation here can be used as the weight to enhance the amplitude of a PT and also to suppress the other high amplitude pixels, such as that from fore-shortening effects or side lobes. In other words, for the pixel with a real PT, the product of its amplitude and the calculated cross-correlation should be much higher than for the other targets.

Before PT detection, we have to set the size of the side lobe truncation when simulating the sinc-like function. Higher truncation leads to a larger number of PT, but the determination of an isolated PT could be less accurate because clutters may decrease over small patches [12]. Ideally, an adaptive truncated pixels patch should be applied according to the texture and patterns of the amplitude image. Nevertheless, as for ASAR data, a good compromise can be achieved by truncating the sinc function to a 11×11 pixel patch. It has to be noticed that the PT detection strategy in our study is different from the one used in coregistration. For instance, in [12], only a small number of pixel-offsets are required to constrain the polynomial mapping function, while we need much more measurements for mapping the coseismic deformation.

To ensure a reasonable distribution of PT on the whole scene, the detection algorithm is performed on overlapping blocks. Pixels with the normalized correlation coefficients between the amplitude patches and sinc function lower than 0.2 are discarded directly. Then, a pixel could be identified as a PT candidate if the product of the correlation coefficient and the amplitude is above an adaptive threshold, which is determined by the mean of the amplitude plus 1.5 times the STD in each block. In this way, the threshold would be loosened if there are not enough high amplitude pixels in some blocks. Afterwards, the locations of each detected PT are used as the input for the pixel-offset tracking.

Offset tracking on PT is similar with the standard one, i.e., the cross-correlation calculation between the master and slave match patches. In our study, we set the reference window as 64×64 pixels. The search window is 8×8 pixels and the correlation oversample factor is 128 (64 in standard method such as the AMPCOR routine of ROI_PAC). Then, the azimuth and range pixel-offset fields, which consist of two components, can be obtained: One comes from the different orbital configurations and the other comes from the displacements occurring between the acquisition time intervals. Empirically, the orbital ramp can be determined by fitting a quadratic polynomial function to the offset fields globally, assuming that there exists no displacement for most parts of the image. Then, pixel offsets caused by displacements can be extracted after the removal of orbital offsets.

It is noticeable that large surface displacements may bias the polynomial coefficients. Moreover, the selected PT candidates may not be the ideal point-like scatterers since the detection is only based on one single image. Therefore, it is still questionable if one can apply the entire set of PT for fitting the orbital ramp coefficients. In order to remove the orbital component in the best possible way, the quadratic polynomial coefficients are obtained from the reference PT after a culling procedure that is dependent on a quadratic model test [14]. Afterwards, the inverted quadratic polynomial coefficients are used to remove the orbital ramp for all PT candidates. It is important to notice that many culled PT are near the coseismic rupture areas, and large displacements are the main reason that they are unable to pass the model test. Therefore, this culling procedure is only applied to fit the orbital offsets but is not used for the removal of pixel-offset outliers.

Now we are at the point of removing outliers among the detected PT. Usually, cross-correlation is considered to retrieve the final prominent PT. Besides, the variances of the cross-correlation surfaces between each match-patch pair can be regarded as the estimations of matching quality [15]. The corresponding histograms can assist us to determine proper thresholds when masking out the unreliable pixel-offset measurements. We will discuss the thresholds in the next section, according to the case study in this paper.

III. Application on 2010 El Mayor−Cucapah Earthquake

A. Seismic Background and SAR Data

The M 7.2 El Mayor–Cucapah earthquake on April 4, 2010 struck northern Baja California, Mexico, USA at a shallow depth along the principal transform boundary between the

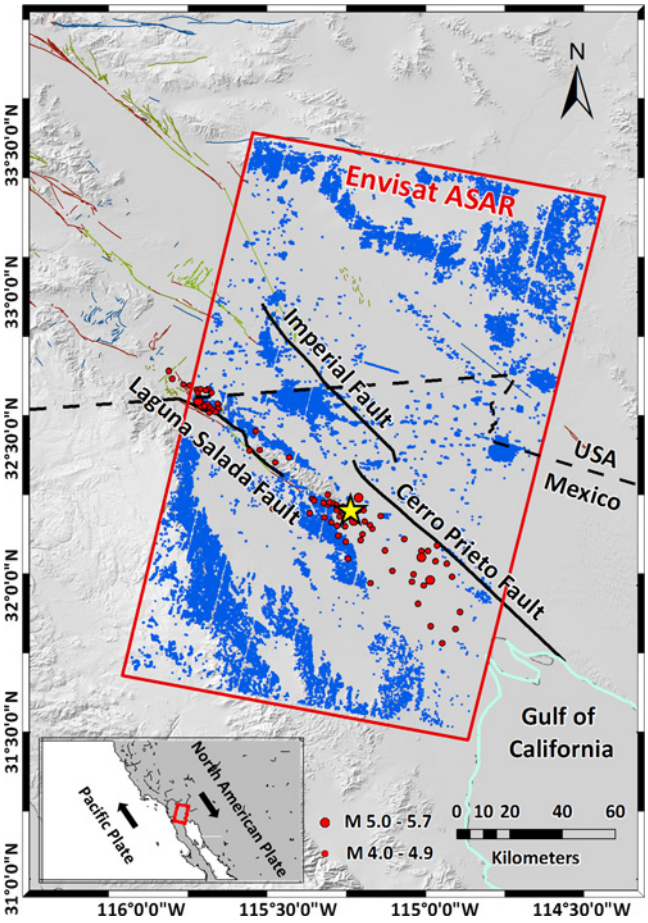

Fig. 1. Setting of the 2010 El Mayor–Cucapah earthquake. The background is the shaded topography of the region. The yellow star is the epicenter. Red circles show aftershocks with magnitude higher than 4.0 as of May 3, 2010. Smaller red circles are M 4.0–4.9, and bigger red circles are M 5.0–5.7. Thin lines indicate all history quaternary faults in this region and the three main faults are represented with black solid lines. Red box shows the track of the ASAR data used. Small blue points depict the distribution of the prominent PT with pixel-offset measurements.

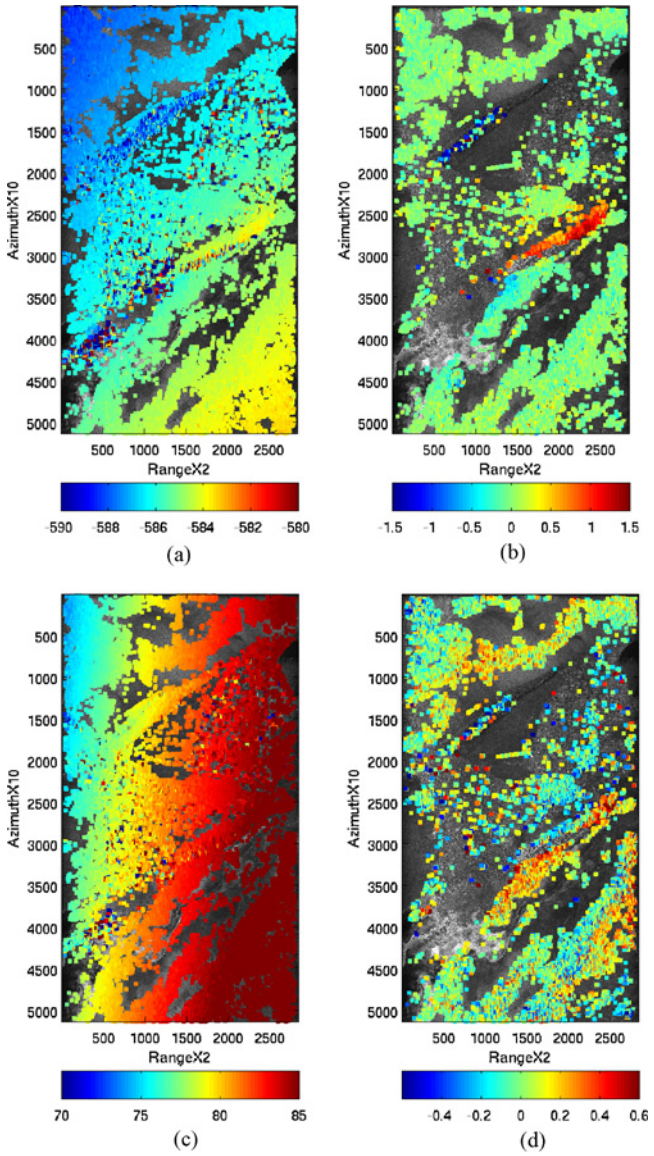

Fig. 2. (a) Original PT candidates and (b) prominent PT offset fields in azimuth. (c) Original PT candidates and (d) prominent PT offset fields in range. Color of PT indicates offsets in meters.

North American and Pacific plates (Fig. 1). As of May 3, 2010, 784 aftershocks with a magnitude equal to or exceeding 3.0, occurred along the 120 km rupture from the south end of the Elsinore fault zone to the northern tip of the Gulf of California (red dots in Fig. 1). Triggered slip occurred on numerous northwest-striking faults with right-lateral slip in the Imperial Valley [16]. Most ruptures lie in high, dry, and remote terrain where few Global Positioning System (GPS) measurements exist. Therefore, remote sensing techniques such as differential Light Detection and Ranging (LIDAR) and InSAR were used to map the surface rupture and to identify extensive liquefactions in the surrounding agricultural areas [16], [17]. Wei *et al.* [18] applied pixel-offset tracking with SAR amplitude images and optical SPOT panchromatic images as well as geodetic and seismological data to reconstruct the fault geometry and slip history.

Here, we implemented the proposed PT offset tracking on a pair of descending ENVISAT ASAR data (Table I). Three of the highest slip-rate faults (∼35–40 mm/year) of the San Andreas Fault system (Laguna Salada Fault, Imperial Fault, and Cerro Prieto Fault) are also covered in this scene (Fig. 1).

TABLE I
BASIC PARAMETERS OF SAR DATA

	Date	Track	Direction	B_t (days)	B_{prep} (m)
Envisat ASAR	20100328 20100502	084	Des.	35	−88

B. Results and Discussion

Using the presented PT detection algorithm, 141 146 PT candidates are initially selected from the master image (51 408 × 5681 pixels). Fig. 2(a) and (c) shows the azimuth and range offsets, respectively. The orbital ramps existing in the entire scenes are clearly visible. It is worth to mention that the pixel offsets in the range direction include a topographic component. When the perpendicular baseline is large, this effect is especially noticeable in the areas of steep topography. Since in our study, the baseline is so small that the topographic effect can be ignored comparing with coseismic displacements. Nevertheless, this component along with the orbital ramp can

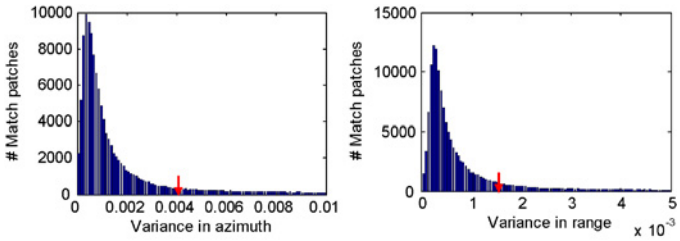

Fig. 3. Variance distributions of the cross-correlation surfaces on the detected PT match patches in (a) azimuth and (b) range directions.

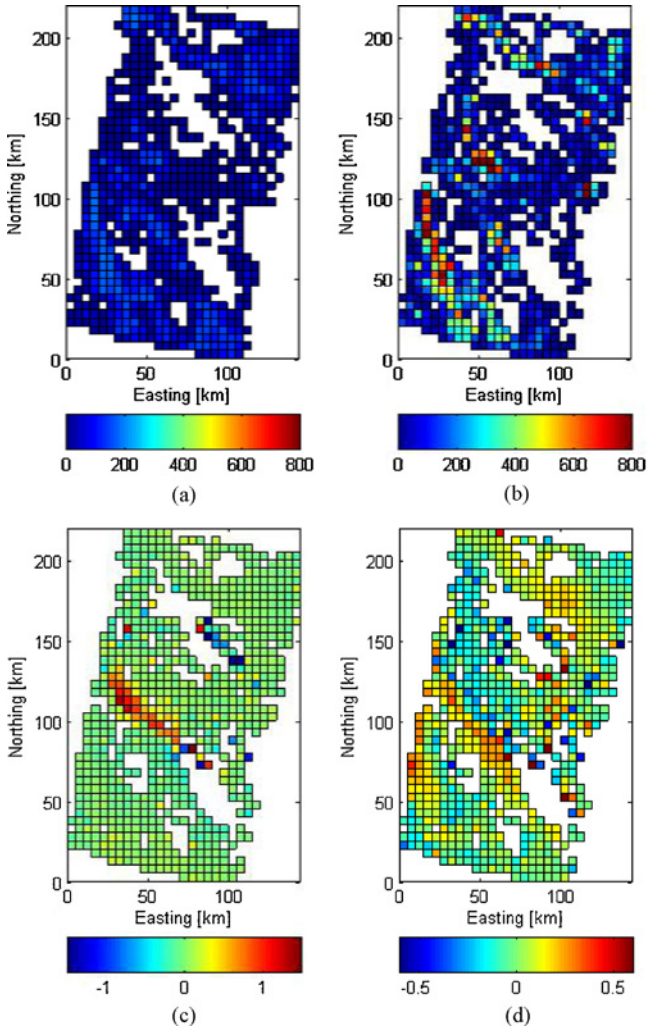

Fig. 4. Comparison between the number of the prominent match patches of (a) standard and (b) PT offset tracking in subsampled grids. In (a) and (b), the color bar indicates the number of measurements in each 5 km × 5 km block. (c) and (d) Subsampled azimuth and range offsets from PT offset tracking in meters. In (c) and (d), the color bar indicates offsets in meters.

be also calculated from the orbit information and topographic data [19].

According to Fig. 3(a) and (b), the maximum variations of azimuth and range cross-correlation surfaces are set as 0.004 and 0.0015. Meanwhile, outliers can be further removed by setting the minimum cross-correlation as 0.45. Fig. 2(b) and (d) shows the remaining offsets of the prominent 93 909 PT (blue dots in Fig. 1). A clear discontinuity can be seen along the main rupture (middle-right red) in the azimuth offset field. Destructive movements in the main rupture, vegetation coverage in the north, and the liquefaction zone in the southeast of the epicenter bounded by the Cerro Prieto Fault lead to sparse/nonexistent PT (Fig. 1). According to [18], these vacant regions also exist for the standard method.

From Figs. 1 and 2(b) and (d), the northeast and southwest sides moved to the opposite directions along the descending ASAR track. The clear asymmetry of near-surface strain with respect to the rupture plane indicates the complex fault geometry. The approximate northwest endpoint of the rupture is located at 32°37′N,−115°45′W, and the rupture extended for ∼60 km on a S36°E orientation to the southeast of the epicenter, which is consistent with the field report in [20].

Besides, pixel offsets in the sand dunes east of the Imperial Valley, which is usually called Algodones Dunes [the blue dots in the top-left of Fig. 2(b)], are distinctive with displacements in the opposite direction to the main rupture. However, as far as we know, this dune regions were not involved or got masked in previous studies using SAR data [16], [18], and the anomalous motion has not been addressed. According to the coherence and amplitude maps, the regions show almost completely incoherence while some pixels reveal high amplitude with regular strip patterns. The surface shifts show dune migrations as a complex consequence of wind, pressure, seismic activities, etc. It can be of interest for geomorphologists using the proposed method to study sand motion, as sand dunes often have strong PT due to its shape [21].

C. Comparisons

It is well-known that in coseismic study, it is unfeasible to involve all the SAR measurements in the geophysical inversion since the forward model computation is expensive. As a consequence, the measurements, i.e., interferogram and/or pixel offsets have to be subsampled before inversion [22]. We compared the standard and PT offset tracking methods using the median subsampled results. In order to simulate the same conditions for the two methods, we applied the similar number of original match-patch candidates (∼141 140) and the same thresholds for the outlier removal. To be more precise, the measurement intervals are ∼100 pixels in azimuth and ∼20 pixels in range for the standard method. After removing outliers, the number of the remaining prominent points was decreased significantly by 72.4% to 38 945 for standard method, and decreased only by 33.5% to 93 909 for PT method.

Fig. 4(a) and (b) shows the number of prominent match patches in subsampled grids (5 km × 5 km) from standard and PT offset tracking. The distributions of the prominent match patches of the two methods are well consistent. However, it is clear that a larger number of prominent match patches could be drawn from PT offset tracking. It is noticeable that we cannot obtain any measurements in some decorrelated areas from the standard or PT methods. One may argue that if we narrow the match-patch intervals in the standard method, we may get some measurements in the blank areas. However, we can also achieve this by loosening the thresholds in the PT detection step and that will be more efficient than introducing a huge number of match patches by increasing their density for the whole image. Moreover, from previously published results such as in [18], these blank areas exist as well in the subsampled offset fields.

According to Fig. 4(c) and (d), the horizontal motions in azimuth are straightforward, i.e., the block on the opposite side moving to the right, as expected. The horizontal offsets are largest near the main rupture, where the maximum

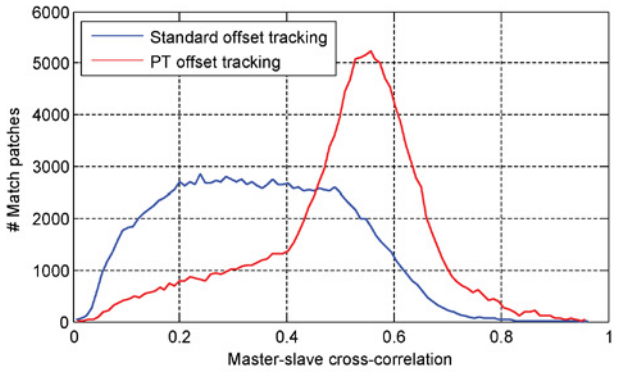

Fig. 5. Master-slave cross-correlation comparison.

displacements of the two plates are 1.5 m and +0.5 m along the track, i.e., with a relative ∼2 m right-lateral slip. While the range offsets fields reveal mostly vertical displacements due to the 23° incidence angle, and the displacements of normal faulting pattern are distinctive, with a relative ∼1 m dip-slip. Overall, the right-lateral slip with an east-side down movements along the plate boundary fault system can also be drawn, adhering to the focal mechanisms of the earthquake.

We also compare the cross-correlation of the match-patches between standard and PT offset tracking. It is noticeable that the cross-correlation algorithm was used twice in our study, one is applied between the master image patches and the simulated sinc function (master-sinc) for PT detection, and the other is applied between the match patches of master and slave images (master-slave) for pixel offset calculation. Fig. 5 shows the master-slave cross-correlation histograms of initial PT candidates by the standard in blue and PT offset tracking in red. The blue line follows a nearly uniform distribution between 0.2 and 0.5, while the red line follows a Gaussian distribution. The sharper the peak is, the more robust the cross-correlation is and more precise the offsets would be [15]. As expected, the cross-correlation obtained from detected PT match patches shows a clear peak near 0.55, indicating that the number of high cross-correlation measurements increase significantly by using PT offset method, and should lead to more accurate displacement measurements.

IV. Concluding Remarks

Standard offset tracking method is an important complement to obtaining large surface displacements in both azimuth and range dimensions where InSAR technique is unfeasible due to excessive displacement gradients and phase unwrapping errors. In order to improve the reliability as well as the efficiency of the standard method, we proposed a simple strategy that focuses on the prior-detected PT match patches. At the same time, orbital ramp can be fitted more accurately with the coefficients calculated from reference PT. The application on the 2010 M 7.2 El Mayor–Cucapah earthquake shows that higher amplitude cross-correlation on PT match patches can be achieved compared with standard method, resulting in more reliable offset estimations. The results may help us better understand the simultaneous normal and right-lateral strike-slip pattern in this seismic event.

Acknowledgments

The authors would like to thank Dr. T. Balz for proofreading the manuscript and two anonymous reviewers for their valuable suggestions.

References

[1] N. B. D. Bechor and H. A. Zebker, "Measuring 2-D movements using a single InSAR pair," *Geophys. Res. Lett.*, vol. 33, p. L16311, Aug. 2006.

[2] R. Michel, J. P. Avouac, and J. Taboury, "Measuring ground displacements from SAR amplitude images: Application to the Landers earthquake," *Geophys. Res. Lett.*, vol. 26, no. 7, pp. 875–878, Apr. 1999.

[3] Z. H. Li, P. Pasquali, A. Cantone, A. Singleton, G. Funning, and D. Forrest, "MERIS atmospheric water vapor correction model for wide swath interferometric synthetic aperture radar," *IEEE Geosci. Remote Sens. Lett.*, vol. 9, no. 2, pp. 257–261, Mar. 2012.

[4] T. A. Scambos, M. J. Dutkiewicz, J. C. Wilson, and R. A. Bindschadler, "Application of image cross-correlation to the measurement of glacier velocity using satellite image data," *Remote Sens. Environ.*, vol. 42, no. 3, pp. 177–186, Dec. 1992.

[5] Y. Fialko, "Probing the mechanical properties of seismically active crust with space geodesy: Study of the coseismic deformation due to the 1992 Mw7.3 Landers (southern California) earthquake," *J. Geophys. Res.*, vol. 109, p. B03307, Mar. 2004.

[6] R. Bamler and M. Eineder, "Accuracy of differential shift estimation by correlation and split-bandwidth interferometry for wideband and Delta-k SAR systems," *IEEE Geosci. Remote Sens. Lett.*, vol. 2, no. 2, pp. 151–155, Apr. 2005.

[7] R. F. Hanssen, *Radar Interferometry: Data Interpretation and Error Analysis*. Norwell, MA, USA: Kluwer Academic Publishers, 2001.

[8] M. Simons, Y. Fialko, and L. Rivera, "Coseismic deformation from the 1999 Mw 7.1 Hector Mine, California, earthquake as inferred from InSAR and GPS observations," *Bull. Seism. Soc. Am.*, vol. 92, no. 4, pp. 1390–1402, May 2002.

[9] S. Jónsson, H. Zebker, and F. Amelung, "On trapdoor faulting at Sierra Negra volcano, Galápagos," *J. Volcanol. Geotherm. Res.*, vol. 144, pp. 59–71, Jun. 2005.

[10] Y. Fialko, M. Simons, and D. Agnew, "The complete (3-D) surface displacement field in the epicentral area of the 1999 Mw7.1 Hector Mine earthquake, California, from space geodetic observations," *Geophys. Res. Lett.*, vol. 28, no. 16, pp. 3063–3066, Aug. 2001.

[11] T. Wang, S. Jónsson, and R. F. Hanssen, "Coregistration between SAR image subsets using pointwise targets," presented at the Fringe 2011 Workshop, Frascati, Italy, Sep. 18–23, 2011.

[12] F. Serafino, "SAR image coregistration based on isolated point scatterers," *IEEE Geosci. Remote Sens. Lett.*, vol. 3, no. 3, pp. 354–358, Jul. 2006.

[13] A. Ferretti, C. Prati, and F. Rocca, "Permanent scatterers in SAR interferometry," *IEEE Trans. Geosci. Remote Sens.*, vol. 39, no. 1, pp. 8–20, Jan. 2001.

[14] B. M. Kampes, R. F. Hanssen, and Z. Perski, "Radar interferometry with public domain tools," presented at the FRINGE 2003 Workshop, Frascati, Italy, Dec. 1–5, 2003.

[15] F. Casu, A. Manconi, A. Pepe, and R. Lanari, "Deformation time-series generation in areas characterized by large displacement dynamics: The SAR amplitude pixel-offset SBAS technique," *IEEE Trans. Geosci. Remote Sens.*, vol. 49, no. 7, pp. 2752–2763, Jul. 2011.

[16] M. Wei, D. Sandwell, Y. Fialko, and R. Bilham, "Slip on faults in the Imperial Valley triggered by the 4 April 2010 Mw 7.2 El Mayor–Cucapah earthquake revealed by InSAR," *Geophys. Res. Lett.*, vol. 38, p. L01308, Jan. 2011.

[17] M. E. Oskin, J. R. Arrowsmith, A. H. Corona, A. J. Elliott, J. M. Fletcher, E. J. Fielding, P. O. Gold, J. J. G. Garcia, K. W. Hudnut, L. Z. Jing, and O. J. Teran, "Near-field deformation from the El Mayor–Cucapah earthquake revealed by differential LIDAR," *Science*, vol. 335, no. 6069, pp. 702–705, Feb. 2012.

[18] S. J. Wei, E. Fielding, S. Leprince, A. Sladen, J. P. Avouac, D. Helmberger, E. Hauksson, R. Chu, M. Simons, K. Hudnut, T. Herring, and R. Briggs, "Superficial simplicity of the 2010 El Mayor–Cucapah Earthquake of Baja California in Mexico," *Nat. Geosci.*, vol. 4, pp. 615–618, Jul. 2011.

[19] E. Pathier, E. J. Fielding, T. J. Wright, R. Walker, B. E. Parsons, and S. Hensley, "Displacement field and slip distribution of the 2005 Kashmir earthquake from SAR imagery," *Geophys. Res. Lett.*, vol. 33, p. L20310, Oct. 2006.

[20] SCSN. (2010, May 10). Mw 7.2 El Mayor–Cucapah Earthquake (Northern Baja California Earthquake) [Online]. Available: http://www.scsn.org/2010sierraelmayor.html

[21] N. T. Bridges, F. Ayoub, J-P. Avouac, S. Leprince, A. Lucas, and S. Mattson, "Earth-like sand fluxes on Mars," *Nature*, vol. 485, pp. 339–342, May 2012.

[22] R. B. Lohman and M. Simons, "Some thoughts on the use of InSAR data to constrain models of surface deformation: Noise structure and data downsampling," *Geochem. Geophys. Geosyst.*, vol. 6, no. 1, Jan. 2005.